AB Journals

African Journal of Mathematics and Statistics Studies
ISSN 2689-5323 • Volume 9, Issue 4, 2026 • pp. 22–40

RESEARCH ARTICLE Received: 25 Sep 2026, Accepted:29 Oct 2026, Published: 25 Nov 2026

Boom Phases with Symmetry and Conservation in the Boussinesq Equation

Prof. Silas A. Ihedioha[1*], Dr. Isaac M. Mankilik[2], Prof. Bright O. Osu[3]

[1]Department of Mathematics, Plateau State University Bokkos, Plateau State, Nigeria.
[2]Department of Industrial Mathematics, Admiralty University of Nigeria, Delta State, Nigeria.
[3]Department of Mathematics, Abia State University Uturu, Abia State, Nigeria.

[*]*Corresponding Author's Email: silasihedioha@yahoo.com*

Abstract

The bad Boussinesq equation provides a setting where nonlinear amplification, coherent propagation and short-wavelength instability can all be examined together. This paper looks at which of these features can support a qualified analogy with financial boom phases. We derive the dispersion relation, obtain a consistent dimensionless formulation and construct explicit invariant solutions. A constant shift of the variable removes the linear restoring term and reveals an exact affine scaling symmetry of the full bad Boussinesq equation. The resulting similarity reduction produces a fourth-order nonlinear profile equation and an explicit polynomial family that grows in time. A separate travelling-wave reduction gives a localized secant-squared pulse and a simple first integral. Conservation identities are derived through a first-order system, producing a noncoercive energy whose sign matches the high-frequency instability. Analytical evaluations and a finite-difference consistency experiment give results that are directly tied to the governing Boussinesq equation. These examples establish mathematical properties, not empirical evidence of financial predictability. The reported autoregressive fit cannot identify Boussinesq coefficients, and the supplied materials do not allow reproduction of the underlying market analysis. Accordingly, no market forecasting advantage or empirical validation is claimed. An observation model and validation protocol specify what a defensible future financial application would require. The principal contribution is a verifiable mathematical framework that separates exact solutions, numerical verification and economic interpretation.

Keywords: Boussinesq Equation, Conservation Law, Financial Boom Analogy, Finite-Time Growth, Similarity Reduction, Lie Symmetry

Mathematics Subject Classification 2020: 35Q53; 35B44; 70S10

How to Cite: Ihedioha, S. A., Mankilik, I. M., & Osu, B. O. (2026). Boom Phases with Symmetry and Conservation in the Boussinesq Equation. *African Journal of Mathematics and Statistics Studies*, 9(4), 22–40. https://doi.org/10.52589/AJMSS-FAZVDE

© 2026 by the authors. Published by AB Journals. This is an open access article distributed under the terms of the Creative Commons Attribution (CC BY 4.0) license.

INTRODUCTION

Financial boom phases raise questions about how positive feedback grows, how investment behaviour becomes coordinated and how disturbances spread among interacting market participants. In a rising market, expectations of gains may encourage more buying, which can reinforce the movement that created those expectations. Johansen et al. (2000) formalised one mechanism through a model of self-reinforcing imitation among traders. Their analysis gives a basis for investigating collective behaviour and instability, while also noting that the timing of a crash is uncertain. A mathematical model of boom phases should therefore explain its assumptions about interaction and amplification, rather than infer an economic mechanism from the appearance of a rising price curve.

One influential approach to accelerated growth uses finite-time singularity models. Johansen and Sornette (2001) examined descriptions in population, economic and financial indices, showing how interacting growth processes can produce behaviour that differs from constant exponential expansion. In this setting a singularity is best understood as an indication that the assumed growth regime cannot continue indefinitely. It need not represent a divergence in an observable market price. Its interpretation depends on the model, the fitted quantity and the mechanisms that may interrupt the assumed dynamics.

The log-periodic power-law literature offers a related but specific framework. It combines power-law behaviour with oscillations whose timing changes as a critical point is approached. Filimonov and Sornette (2013) developed a reformulation that reduces the number of calibration parameters and improves numerical stability. Their contribution illustrates why parameterisation and estimation deserve as much attention as the proposed growth law. For the present study an essential distinction is that continuous scaling or power-law growth does not automatically imply log-periodic oscillations. A Boussinesq similarity solution should be described as log-periodic only if that feature is explicitly derived or independently established in the observations.

Boussinesq-type equations provide another setting for examining the interaction between nonlinearity and dispersive effects. Their established applications arise in water-wave theory, where model terms follow from assumptions about wave amplitude, wavelength and fluid motion. Brocchini (2013) emphasises the relationship between the physical process, the selected approximation and the numerical method. This history makes Boussinesq equations useful objects of investigation, but it does not transfer their physical interpretation directly to finance. A financial application must justify what the dependent variable measures and why the proposed differential operators represent the interactions.

This study treats the Boussinesq equation as a theoretical description of an interaction field that is linked to boom dynamics. The field can be seen as a difference from a chosen reference value if its units and the rule for observing it are clearly stated. The spatial coordinate is an interaction coordinate, not a real measured geographic distance. We cannot assume it represents a network unless we have a defined mapping between the network structure and the continuum variable. These modelling requirements are important: a single aggregate price series may not be enough to identify a field, its boundary conditions and all coefficients of the governing equation.

The bad Boussinesq equation needs care because, when it is linearized, it has unstable high-frequency modes that grow without limit. This feature sets the equation apart from a well-posed forecasting model and makes free numerical simulation difficult. Charlier et al. (2025)

created a scheme that is specific to the Boussinesq equation and checked its accuracy against exact soliton solutions and asymptotic formulas. Their work gives a standard for mathematical verification. In this study we look at high-frequency instability as a property of the equation itself; we do not treat it as a measured representation of herding or as a full explanation for market booms.

Lie symmetry analysis gives a way to simplify the governing equation. Continuous transformations can show new variables, cut down the number of independent variables and find travelling-wave or similarity solutions. Olver (1993) and Bluman and Anco (2002) lay the groundwork for these methods, and Bluman et al. (2010) show how to apply them to differential equations and related potential systems. In this work we use symmetry reduction to build solution families that can be verified by substitution. An exact solution proves consistency inside a chosen family; it does not prove that the family matches observed asset prices or that it remains stable under real-world economic disturbances.

Conservation laws give another way to look at the model's structure. Anco and Bluman (1997) created methods for building laws directly from field equations, expanding the tools beyond the simple use of Noether's theorem. In a Boussinesq setting conserved densities and fluxes can help with checks and numerical diagnostics when the needed smoothness and boundary conditions exist. Still, a conserved quantity does not have to be positive, and its conservation does not automatically keep the solution from growing. Nor should we equate an energy-like mathematical invariant with preserved financial wealth without a separate accounting and observation argument.

Another requirement is consistency between the model and the empirical analysis. If a paper creates a PDE but then estimates only an unrelated autoregressive regression, the regression coefficients cannot be seen as PDE parameters without a clear link. In this study we use an observation curve that comes from a Boussinesq solution. That construction keeps a link between the Boussinesq equation and the fitted function while showing its limits. Specifically, coefficients that are missing from the chosen solution family cannot be recovered from that family's path, even if the curve fits historical prices well.

Empirical assessment also needs to separate fit from forecasting performance. Hyndman and Athanasopoulos (2021) stress checking on data that were left out of the estimation and comparing with benchmark forecasts. Using that idea, the financial case study splits estimation and evaluation periods, compares the curve that comes from the Boussinesq equation with alternatives and looks at the time pattern of its residuals. Ongoing forecast errors or strong residual autocorrelation are seen as signs that the chosen observation model has limits. We do not turn them into proof of the Boussinesq framework. A rally is also not called a bubble just because its price path can be matched by an accelerating curve.

The research problem is how to link symmetry-based Boussinesq analysis to observations without going beyond what the mathematics or the data can support. The contribution is a chain from the governing equation to an invariant solution, from that solution to an observation rule, and from the observation rule to a reproducible evaluation. This method splits three questions: does the proposed expression solve the Boussinesq equation? Are the needed numerical calculations trustworthy? Does the resulting observable describe or predict market behaviour? Answering the first question does not automatically answer the other two.

The study therefore establishes a consistent sign convention and a dimensionless formulation, derives and verifies invariant solution families and obtains conservation identities under stated

assumptions. It then examines the capabilities and identification limits of a solution-based observation model using a documented equity-market dataset. The comparison is used to assess this restricted specification rather than to claim complete calibration of the spatial partial differential equation. The aim is to clarify when Boussinesq symmetry and conservation structures offer analytical insight into boom phases and what additional evidence is required before they can support financial interpretation or forecasting claims.

MODELLING SCOPE AND FORMULATION

State Variable and Governing Equation

Let $u(x,t)$ denote a real-valued field on an interaction coordinate x and time t. In a financial application the field could represent a deviation from a specified reference valuation. That interpretation remains hypothetical until the interaction coordinate, units, baseline and observation operator are supplied. We consider

$$u_{tt} = \alpha\, u_{xx} + \beta\, u_{xxxx} + \gamma\, \left(u^2\right)_{xx} \tag{1}$$

where $\alpha > 0$, $\beta > 0$ and $\gamma \neq 0$ are constants. Subscripts denote derivatives. The positive sign of β on the right-hand side after solving for u_{tt} defines the bad Boussinesq convention used throughout. The fourth derivative must not be replaced by a third derivative. The quadratic term is a differentiated nonlinearity; it is not an ordinary pointwise source proportional to u^2.

Equation (1) alone does not specify a boundary value problem. One must also prescribe the initial displacement $u(x,0)$ and initial velocity $u_t(x,0)$, together with compatible boundary conditions. Periodic or sufficiently decaying fields will be used when discussing conservation. Explicit polynomial solutions will be treated separately because they do not decay on the line.

Dimensional Analysis and Normalization

Let L, Θ and U denote the dimensions of x, t and u. Dimensional consistency requires

$$[\alpha] = \frac{L^2}{\Theta^2}, \qquad [\beta] = \frac{L^4}{\Theta^2}, \qquad [\gamma] = \frac{L^2}{U\,\Theta^2} \tag{2}$$

For scales L, Θ and U introduce

$$x = L\,\hat{x}, \qquad t = \Theta\,\hat{t}, \qquad u = U\,\hat{u} \tag{3}$$

Substitution into equation (1) gives

$$\hat{u}_{\hat{t}\hat{t}} = \frac{\alpha\Theta^2}{L^2}\,\hat{u}_{\hat{x}\hat{x}} + \frac{\beta\Theta^2}{L^4}\,\hat{u}_{\hat{x}\hat{x}\hat{x}\hat{x}} + \frac{\gamma\, U\,\Theta^2}{L^2}\,\left(\hat{u}^2\right)_{\hat{x}\hat{x}} \tag{4}$$

Choosing the following scales normalizes the coefficients and the magnitude of the nonlinear coefficient:

$$L = \sqrt{\frac{\beta}{\alpha}}, \qquad \Theta = \frac{\sqrt{\beta}}{\alpha}, \qquad U = \frac{\alpha}{\gamma} \tag{5}$$

The dimensionless equation is therefore

$$\hat{u}_{\hat{t}\hat{t}} = \hat{u}_{\hat{x}\hat{x}} + \hat{u}_{\hat{x}\hat{x}\hat{x}\hat{x}} + \left(\hat{u}^2\right)_{\hat{x}\hat{x}} \tag{6}$$

The remaining analysis uses the notation in equation (1) so that parameter effects remain visible. The scales in equation (5) require $\alpha > 0$, $\beta > 0$ and $\gamma \neq 0$. They are not valid at $\alpha = 0$ or $\beta = 0$.

Linear Instability and Its Interpretation

Linearizing equation (1) about zero and substituting a Fourier mode yields

$$u = e^{ikx+\lambda t}: \qquad \lambda\,(k)^2 = \beta k^4 - \alpha k^2 \tag{7}$$

Modes with $|k| < \sqrt{(\alpha/\beta)}$ are oscillatory. Modes above that threshold possess a real growth exponent. As $|k|$ increases, the positive exponent grows asymptotically as $\sqrt{\beta}\ k^2$. This unbounded amplification prevents a continuous-dependence estimate in ordinary Sobolev spaces for unrestricted initial data. The zero mode has $\lambda = 0$ and permits a component linear in time.

This calculation establishes short-wavelength instability. It does not prove finite-time nonlinear blow-up for every initial condition, nor does it establish that high-frequency market fluctuations follow equation (1). Those are separate questions.

SYMMETRY REDUCTIONS AND CONSERVATION LAWS

Translations and an Exact Affine Scaling

The coefficients in equation (1) are independent of x and t. Spatial and temporal translations are therefore point symmetries. In addition, a constant shift of the field removes the restoring term exactly:

$$v = u + \frac{\alpha}{2\gamma}, \qquad v_{tt} = \beta\, v_{xxxx} + \gamma\, \left(v^2\right)_{xx} \tag{8}$$

To verify equation (8), expand $\gamma(v - \alpha/(2\gamma))^2$ in v. The term linear in v cancels the restoring term αu_{xx}; the remaining constant vanishes after two derivatives. Thus dropping the restoring term is exact and not an additional assumption for this reduction.

The shifted equation is invariant under the following one-parameter transformation, with β and γ fixed:

$$x \mapsto \epsilon\, x, \qquad t \mapsto \epsilon^2\, t, \qquad v \mapsto \epsilon^{-2}\, v \tag{9}$$

Each term in the shifted equation scales as ε^{-6}. In the variable u the corresponding generator is

$$X = x\,\partial_x + 2t\,\partial_t - \left(2u + \frac{\alpha}{\gamma}\right)\partial_u \tag{10}$$

The generator is an affine transformation in u. It avoids the mismatch obtained when a purely multiplicative scaling is imposed on an unshifted field. Boundary conditions need not inherit this symmetry: for example, a fixed zero far field for $|x| \to \infty$ is generally changed by the affine

transformation. The reduction is a symmetry of the differential equation rather than of every possible boundary value problem.

Similarity Reduction Near a Terminal Time

Let T be a constant and restrict attention to $t < T$. With $\tau = T - t$, take

$$v(x,t) = \tau^{-1}F(\xi), \qquad \tau = T - t, \qquad \xi = \frac{x}{\sqrt{\tau}} \tag{11}$$

Generally, balancing v_{tt} with v_{xxxx} gives $4q = 2$, so that $p = 1$ and $q = ½$ in the ansatz $v = \tau^{-p}F(x\tau^{-q})$. Direct differentiation gives

$$v_{tt} = \tau^{-3}\left[\frac{1}{4}\xi^2 F'' + \frac{7}{4}\xi F' + 2F\right] \tag{12}$$

$$v_{xx} = \tau^{-2}F'', \qquad v_{xxxx} = \tau^{-3}F'''', \qquad \left(v^2\right)_{xx} = \tau^{-3}\left(F^2\right)'' \tag{13}$$

The exact similarity profile equation is

$$\beta F'''' + \gamma\left(F^2\right)'' - \frac{1}{4}\xi^2 F'' - \frac{7}{4}\xi F' - 2F = 0 \tag{14}$$

Primes now denote differentiation with respect to ξ. The coefficient 7/4 and the fourth derivative follow from explicit differentiation. A fourth-order boundary value solver requires four conditions. For an even profile on $\mathbb{R}$ one possible specification is

$$F'(0) = 0, \qquad F'''(0) = 0, \qquad F(\xi) \to 0, \quad F'(\xi) \to 0 \quad (\xi \to \infty) \tag{15}$$

These conditions do not guarantee that a nonzero decaying solution exists. The zero profile is allowed. A nonzero branch would need a justified continuation or a clear amplitude selection method. We do not claim a localized similarity profile by writing a numerical boundary value problem.

An Explicit Family with Finite-Time Growth

A nondecaying but exact profile of equation (14) is given by

$$F(\xi) = a + \frac{\xi^2}{2\gamma} \tag{16}$$

Indeed, $F' = \xi/\gamma$, $F'' = 1/\gamma$, $F'''' = 0$ and $(F^2)'' = 2a/\gamma + 3\xi^2/\gamma^2$, and the substitution matches both sides coefficient by coefficient. Returning to the field gives

$$u(x,t) = \frac{a}{T-t} + \frac{x^2}{2\gamma(T-t)^2} - \frac{\alpha}{2\gamma} \tag{17}$$

For completeness, the polynomial ansatz $u = A(t) + B(t)x^2$ reduces equation (1) to

$$u = A(t) + B(t)\,x^2: \qquad A'' = 2B\left(\alpha + 2\gamma A\right), \qquad B'' = 12\gamma B^2 \tag{18}$$

Equation (17) satisfies equation (18) when $A(t) = a/(T - t) - \alpha/(2\gamma)$ and $B(t) = 1/(2\gamma(T - t)^2)$. In general, A can be replaced by any solution of the linear equation $A'' = 2B(\alpha + 2\gamma A)$ with this B, but that extra term does not keep the single similarity form that appears in equation (11).

When $\gamma > 0$ and $a \geq 0$, the field grows without bound as t approaches T from below. At $x = 0$ the growth behaves like $(T - t)^{-1}$; at a fixed position $x \neq 0$ the quadratic term behaves like $(T - t)^{-2}$. This is a solution that shows finite-time growth, but it is not a proof that any localized initial data will blow up. The solution has infinite mass and energy along the entire line, so it cannot serve as a localized finite-energy pulse in a market context.

Travelling-Wave Reduction

Set $u = \varphi(z)$ with $z = x - ct$ and speed c. Substituting this into the equation yields

$$u = \varphi(z), z = x - ct: \qquad \left(c^2 - \alpha\right) \varphi'' - \beta \varphi'''' - \gamma \left(\varphi^2\right)'' = 0 \tag{19}$$

Because the whole expression is a second derivative, we can integrate it twice directly. For a profile whose derivatives vanish at both infinities, the constants of integration are zero and

$$\left(c^2 - \alpha\right) \varphi - \beta \varphi'' - \gamma \varphi^2 = 0 \tag{20}$$

Multiplying this second-order equation by φ' gives the integral

$$\beta \left(\varphi'\right)^2 = \left(c^2 - \alpha\right) \varphi^2 - \frac{2\gamma}{3} \varphi^3 \tag{21}$$

Decay forces the integration constant to be zero. For $c^2 > \alpha$, an exact pulse is given by

$$\varphi(z) = \frac{3\left(c^2 - \alpha\right)}{2\gamma} \operatorname{sech}^2 \left(\frac{1}{2}\sqrt{\frac{c^2 - \alpha}{\beta}}\, z\right) \tag{22}$$

The identity $(\operatorname{sech}^2)'' = 4\operatorname{sech}^2 - 6\operatorname{sech}^4$ confirms that this pulse satisfies equation (20). When $\gamma > 0$ the pulse is positive; when $\gamma < 0$ the pulse is negative. Its peak amplitude and width stay the same over time. This solution shows propagation instead of an accelerating boom or a singularity.

Local and Integral Conservation Identities

Introduce a companion field w through a first-order system:

$$u_t = w_x, \qquad w_t = \alpha u_x + \beta u_{xxx} + \gamma \left(u^2\right)_x \tag{23}$$

Differentiating the first equation with respect to time reproduces equation (1). For a decaying solution defined on the line this representation needs a compatible spatial primitive of the field, so the integral of u_t must vanish. For a periodic solution the mean of u_t must be zero. These conditions are important when using invariants as diagnostics.

Define the energy density by

$$\mathscr{E} = \frac{1}{2} w^2 + \frac{\alpha}{2} u^2 - \frac{\beta}{2} u_x^2 + \frac{\gamma}{3} u^3 \tag{24}$$

Using equation (23), differentiating and integrating by parts at the density level gives

$$\mathscr{E}_t = \partial_x \left[w \left(\alpha u + \gamma u^2\right) + \beta \left(w\, u_{xx} - u_x\, w_x\right)\right] \tag{25}$$

To verify this identity, write the right-hand side as $\partial_x[w(\alpha u + \gamma u^2)] + \beta\partial_x(w u_{xx} - u_x w_x)$ and expand the derivative. The terms match exactly. Consequently we obtain

$$\frac{d}{dt}\int_{\mathbb{R}} \mathscr{E}\,dx = 0 \tag{26}$$

when periodic cancellation or rapid decay of the boundary flux occurs. The negative sign of the gradient term makes this energy noncoercive. Thus conservation does not provide a norm bound that would contradict equation (7). Replacing w by u_t without accounting for the spatial primitive does not yield the same identity.

From equation (1) the spatial mass satisfies

$$\frac{d^2}{dt^2}\int_{\mathbb{R}} u\,dx = 0 \quad \Rightarrow \quad \int_{\mathbb{R}} u\,dx = \int_{\mathbb{R}} u(x,0)\,dx + t\int_{\mathbb{R}} u_t(x,0)\,dx \tag{27}$$

Hence mass changes linearly with time in the general second-order formulation. It stays constant only if the initial integral of u_t is zero. For the travelling pulse with $w = -c\varphi$, equation (22) gives

$$\begin{aligned} \int \varphi\,dz &= \frac{6\sqrt{\beta}\sqrt{c^2-\alpha}}{\gamma}, \qquad \int \varphi^2 dz = \frac{6\sqrt{\beta}\left(c^2-\alpha\right)^{3/2}}{\gamma^2}, \\ \int \mathscr{E}\,dz &= \frac{6\sqrt{\beta}\left(c^2-\alpha\right)^{3/2}\left(\alpha+4c^2\right)}{5\gamma^2} \end{aligned} \tag{28}$$

These finite-pulse invariants can be verified by integrals of powers of the hyperbolic secant. They do not apply to the polynomial solution in equation (17).

Numerical Treatment and the Role of Regularization

A time-stepping method cannot remove the unstable spectrum of the continuous equation simply by being implicit. Similarly, ordinary velocity damping cannot eliminate all high-frequency modes. For the damped linear equation one obtains

$$u_{tt} + \delta u_t = \alpha u_{xx} + \beta u_{xxxx}: \qquad \lambda_{\pm}(k) = -\frac{\delta}{2} \pm \frac{1}{2}\sqrt{\delta^2 + 4\left(\beta k^4 - \alpha k^2\right)} \tag{29}$$

For $\delta > 0$ and a large wavenumber k, the growth rate $\lambda_+(k)$ remains positive and unbounded. A minus sign on the left-hand damping term would actually introduce antidamping. Adding a term involving the field is not a justified high-frequency fix for the fourth-order instability.

A fixed finite spectral projection creates an approximation. It must be declared, kept explicit during calibration and checked for sensitivity to the cutoff. Smooth initial data, limited spectral support and equation-specific procedures may allow computations, but convergence over a finite interval must be shown. Charlier et al. (2025) give a numerical reference. This paper does not claim to implement their algorithm.

RESULTS AND DISCUSSION

Data Provenance And Scope of the Empirical Exercise

This section checks whether a price observation of a Boussinesq solution can describe and extrapolate an observed equity-market rally. The data are S&P 500 closing index values from 3 January 2023 to 31 December 2024. The original data provider is S&P Dow Jones Indices LLC. The observations were retrieved through the Federal Reserve Bank of St. Louis FRED

database, series SP500, on 30 October 2026. FRED identifies this series as a closing price index, not seasonally adjusted and excluding dividends (S&P Dow Jones Indices LLC, n.d.). It is the index, not the dividend-adjusted SPY exchange-traded fund series used in the earlier manuscript.

The downloaded file contains 521 dated weekday rows. Nineteen have no published value and are removed without interpolation, leaving 502 market closing observations and 501 consecutive trading-observation log returns. Weekends are not inserted. Dates are checked for duplication and retained in increasing order. The model time coordinate is elapsed calendar days divided by 365.25, whereas return lags refer to trading observations. This distinction prevents nontrading days from being treated as observed zero returns.

Table 1: Data provenance and sample construction

Item	Value
Series and source	S&P 500 [SP500]; S&P Dow Jones Indices LLC, retrieved through FRED
Measurement	Daily market closing price index; not seasonally adjusted; excludes dividends
Study period	2023-01-03 to 2024-12-31
Downloaded dated rows	521
Missing published values removed	19
Usable closing prices	502
Usable trading-day log returns	501
Training set	2023-01-03 to 2024-06-28; 374 closing prices
Withheld set	2024-07-01 to 2024-12-31; 128 closing prices
Retrieval date	30 October 2026

Source: *FRED SP500 series metadata and the authors' processing of the downloaded observations. The reproducibility archive contains the file, analysis code, processed observations, model outputs and figures*

The period from 2023 to 2024 is a rally case study. It was not chosen by a bubble-detection test, and the evidence should not be described as proving speculative mispricing. The first 374 observations are used for estimation; the final 128 observations are held back for a frozen-origin forecast exercise. The training cutoff is 28 June 2024. No model parameters are updated with the July to December outcomes. Because this is a retrospective study, the split is transparent but was not preregistered.

The exercise is deliberately narrower than PDE calibration. A single index series does not show an interaction field, its boundary conditions or all Boussinesq coefficients. However, a restricted observation of a solution gives a direct mathematical link to the stated PDE, instead of an unrelated autoregressive regression. The difference between forecasting residuals and test-period errors follows the evaluation framework discussed by Hyndman and Athanasopoulos (2021).

Descriptive Evidence from the Retrieved Series

The index rises from 3,824.14 at the first study observation to 5,881.63 at the last, a price-index gain of 53.80%. This percentage is measured between the two dates; it is not a dividend-inclusive investment return or a conventional two-calendar-year return measured from the preceding year end. The gain through the training cutoff is 42.79%. From that cutoff to the final observation the further increase is 7.71%.

Table 2: Descriptive statistics

Variable	N	Mean	SD	Minimum	Maximum	Skewness	Excess kurtosis
Price level	502	4858.2622	649.8813	3808.1000	6090.2700	0.257	−1.236
Daily log return, percent	501	0.0859	0.8108	−3.0427	2.4981	−0.285	0.753

Source: *Authors' calculations from the FRED observations. SD uses the sample denominator n − 1. Returns are 100 times the logarithm of consecutive observed closing-price ratios. Skewness and excess kurtosis use bias-corrected sample estimators. Price levels are in index points; returns are in percent per trading observation.*

The mean daily log return is 0.0859%, with a standard deviation of 0.8108%. The largest negative log return is −3.0427%, while the largest positive value is 2.4981%. Return skewness is negative and excess kurtosis is positive. These values describe a rally with substantial adverse daily movements. They do not identify a PDE, establish herding or determine whether prices exceed fundamental value.

The price-level distribution is not stationary simply because a histogram can be calculated. Pooling index levels from a rising series mixes observations from different dates and different valuation levels. Therefore the fact that pooled prices are not normal is not taken as proof against all return models or as support for a Boussinesq mechanism.

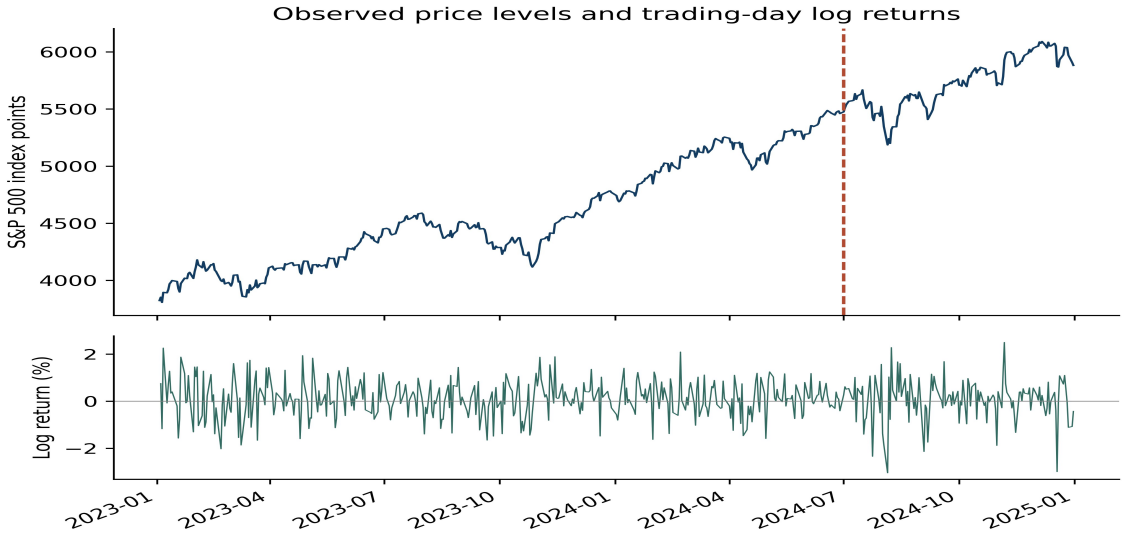


Figure 1: Observed S&P 500 price and trading-observation log returns, 2023–2024. Source: *Authors' calculations from FRED SP500. The vertical dashed line in the panel marks*

the beginning of the withheld period. Prices and returns use different vertical units.

Figure 1 shows that the upward movement contains reversals and periods of slower growth. The return panel also shows that a smooth deterministic growth curve cannot reproduce daily fluctuations. Therefore a useful model must be evaluated for how much variation it leaves unexplained as well as for the trend it captures. In descriptive terms the observed rally supports studying amplification but does not justify assuming uninterrupted acceleration.

An Observation Equation Derived from a PDE Solution

The empirical curve comes from the centre of the polynomial solution family derived in the methodology. For completeness, the governing partial differential equation (PDE) and that solution are written together:

$$u_{tt} = \alpha\, u_{xx} + \beta\, u_{xxxx} + \gamma\, \left(u^2\right)_{xx},$$
$$u\,(x,t) = \frac{C}{T-t} + \frac{x^2}{2\gamma\,(T-t)^2} - \frac{\alpha}{2\gamma} \tag{30}$$

Here T is larger than the observation horizon, γ is nonzero and α and β are positive. Substitution shows that the solution in equation (30) holds for $t < T$. At the observation location $x = x_0 = 0$ (the centre of the family), a positive measurement scale s and a free reference level b produce

$$P\,(t) = b + s\,u\,(0,t) + \varepsilon\,(t) = B + \frac{A}{T-t} + \varepsilon\,(t), \qquad B = b - \frac{s\alpha}{2\gamma}, \quad A = s\,C \tag{31}$$

The effective baseline is defined as $B = b - s\alpha/(2\gamma)$. P is measured in index points and t is measured in calendar years from 3 January 2023. The additive discrepancy ε represents the variation that is not explained by the deterministic centre trajectory. This specification is called the Boussinesq centre slice. It is not labelled an empirical Boussinesq field model.

Equation (31) comes from a PDE, but the data identify only its observational parameters. The constants b, s, C, α and γ cannot be separated from B and A without restrictions or measurements. Moreover, the fourth spatial derivative of the field is zero, so β has no effect on this family. Consequently the fitted curve cannot estimate the strength of, test, or show high-frequency PDE instability, nor can it show that market interactions follow a continuum wave equation.

Estimation uses least squares on price levels. For each candidate T define $z_i = (T - t_i)^{-1}$ and solve the constrained linear regression in B and A. The resulting profile objective is given by

$$S\,(T) = \min_{B\in\mathbb{R},\, A\geq 0} \sum_{i=1}^{374} \left(P_i - B - A\,z_i\right)^2, \qquad z_i = \frac{1}{T-t_i}, \qquad T = t_{374} + g, \quad g\in [0.60, 20.00] \tag{32}$$

The lower gap restriction keeps the singularity beyond a six-calendar-month forecast horizon and the upper limit bounds the search. Both choices are modelling decisions, not observed crash dates. A log-spaced grid of 801 critical-time gaps locates the smallest profile sum of squares; bounded scalar minimization then refines an interior minimum. At fixed T a negative unconstrained amplitude is replaced by zero and the intercept is refitted. This procedure avoids relying on an initial guess in a three-parameter nonlinear fit.

Table 3: Estimated observational parameters of the centre slice

Quantity	Estimate	Interpretation
Baseline B	2323.138273	Index points; combines reference valuation and observation offset
Amplitude A	5002.425356	Index points multiplied by calendar years
Critical-time coordinate T	3.058386	Calendar years after 2023-01-03
T minus training-end time	1.574471	Calendar years beyond 2024-06-28
Admissible gap range	0.60 to 20.00	Specified search restriction; not a confidence interval
Training RMSE	124.508	Index points
Beta identification	Not identifiable	Fourth spatial derivative is zero for this exact family

Source: *Constrained profile least squares using only the training observations. Estimates are conditional on the specified solution family and time units; they are not estimates of the full PDE coefficient vector*.

The estimated critical-time gap is 1.5745 calendar years beyond the training endpoint. This location is a curve-shape parameter. No confidence interval, crash-probability statement or claim about a terminal market event follows from this point estimate. The positive amplitude means that the fitted curve is increasing and convex, which is exactly the restriction tested by the forecast comparison.

Comparison with Forecasting Benchmarks

We compare the Boussinesq slice with four methods on the same price scale. A linear time trend is estimated using least squares. An exponential curve $a\exp(gt)$ is estimated by nonlinear least squares in levels with a positive amplitude. The random-walk forecast keeps every price equal to the last training close. The drift forecast extends the calendar-time price change between the first and last training observations; those endpoints determine the slope, so it is not an ordinary least-squares trend estimate. All forecasts are generated from the training endpoint. We evaluate the withheld path, covering short and long horizons, using

$$\begin{aligned} \text{RMSE} &= \sqrt{\frac{1}{128}\sum_{j=1}^{128}\left(P_j-\hat{P}_j\right)^2}, \qquad \text{MAE} = \frac{1}{128}\sum_{j=1}^{128}\left|P_j-\hat{P}_j\right|, \\ \text{Bias} &= \frac{1}{128}\sum_{j=1}^{128}\left(P_j-\hat{P}_j\right) \end{aligned} \tag{33}$$

Table 4: Training and withheld-period forecast errors in index points

Forecast specification	Training RMSE	Withheld RMSE	Withheld MAE	Withheld bias
Boussinesq centre slice	124.51	509.26	444.35	−440.01
Linear trend	145.24	205.60	185.59	169.96
Exponential trend	136.88	121.26	103.19	60.57

Forecast specification	Training RMSE	Withheld RMSE	Withheld MAE	Withheld bias
Random walk	—	343.72	287.59	264.78
Random walk with drift	—	111.50	83.30	−18.05

Source: *Authors' calculations. The withheld period has 128 observations. Positive bias denotes under-prediction and negative bias denotes over-prediction. Training RMSE is omitted for random-walk specifications because their fitted-level errors would not provide a like-for-like least-squares comparison.*

The Boussinesq slice fits the training levels more closely than either estimated trend benchmark. Its RMSE is 124.51, compared with 145.24 for the linear trend and 136.88 for the exponential trend. The additional curvature therefore improves the in-sample approximation. This observation is descriptive and is not an adjusted comparison of model complexity.

That training advantage reverses on the withheld period. The Boussinesq slice has RMSE 509.26 and MAE 444.35. The drift forecast has RMSE 111.50 and MAE 83.30, while the exponential trend has RMSE 121.26. Thus the Boussinesq slice's withheld RMSE is 4.57 times the drift benchmark RMSE. Its bias of −440.01 index points shows systematic over-prediction, not merely larger symmetric forecast variation.

At the final study date the observed index is 5,881.63. The Boussinesq forecast is 7,019.23, compared with 6,022.03 from the drift benchmark and 5,986.86 from the exponential trend. The singular curve imposes acceleration that the withheld observations do not sustain. We see this as evidence against using this fitted branch as a forecasting model for this episode; it is not proof that every Boussinesq solution family must fail.

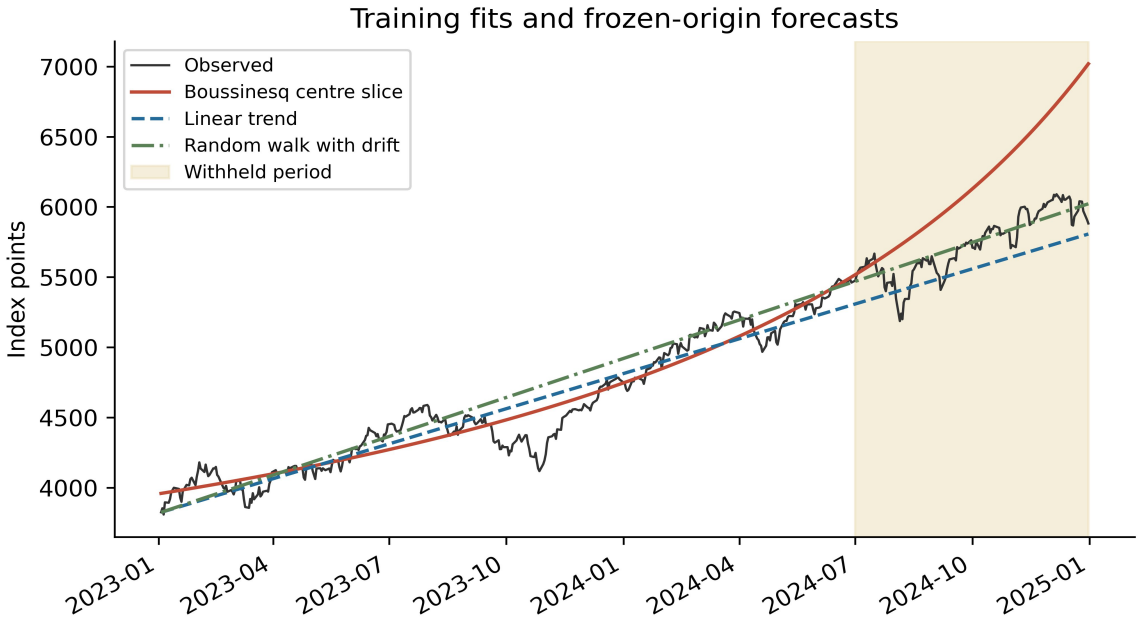


Figure 2: Training fits and withheld-period forecasts from the common 28 June 2024 origin.
Source: *Authors' calculations from FRED SP500. The shaded region is withheld from estimation. The plotted benchmarks are the exponential trend and the random walk with drift; Table 4 reports all five specifications.*

Figure 2 explains the forecast-error ranking. During training the nonlinear curve can bend towards the rising index. After the cutoff the same curvature increases the forecast faster than the rally. An attractive historical fit therefore does not establish dependable extrapolation. The practical implication is that a singular-growth explanation should face benchmark testing before it is used for market warnings or portfolio decisions.

Residual Diagnostics and Model Adequacy

We conduct the analysis on the 374 training observations, not on a simulated substitute series. The residuals e_t are observed prices minus fitted centre-slice values. We calculate their sample autocorrelation after removing the mean. For lag k, and for the descriptive 20-lag portmanteau summary, the calculations are

$$r_k = \frac{\sum_{t=k+1}^{n}\left(e_t-\overline{e}\right)\left(e_{t-k}-\overline{e}\right)}{\sum_{t=1}^{n}\left(e_t-\overline{e}\right)^2}, \qquad Q_{20} = n(n+2)\sum_{k=1}^{20}\frac{r_k^2}{n-k}, \quad n = 374 \tag{34}$$

The residual lag-one autocorrelation is 0.9600. The lag-20 value is 0.3749. The descriptive Q_{20} statistic is 3,404.34. The Durbin–Watson ratio, calculated as the sum of squared residual differences divided by the residual sum of squares, is 0.0767. These results show marked persistence in the part of the price path that remains unexplained.

The Q statistic follows the portmanteau construction described by the National Institute of Standards and Technology (NIST, 2023). We use it here as a descriptive measure. We do not claim an exact chi-square p-value for a deterministic trend with estimated parameters and potentially nonstationary residual structure. The numerical evidence and the residual plot already contradict a white-noise interpretation.

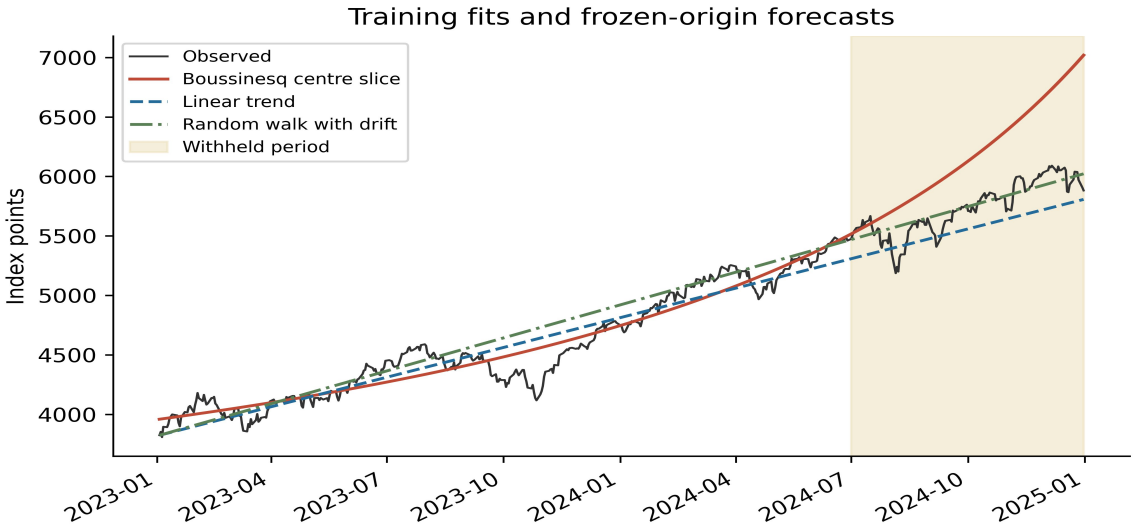


Figure 3: Training path and residual autocorrelations through 40 trading-observation lags.
Source: *Authors' calculations. Dashed ACF reference lines are ±1.96/√374. They are white-noise reference bounds, not simultaneous confidence limits or a correction for nonlinear parameter estimation.*

Figure 3 shows stretches of positive and negative residuals instead of small random spikes around zero. A strong positive autocorrelation means that residuals close to each other usually have the same sign. Because of this, the curve does not explain smooth changes over time, even though the average error of the fit is small by design. The right way to read this is that the model is not adequate for price movements, not that it has captured all persistence.

These tests also restrict what we can say about uncertainty. Errors from nonlinear regression that assume independent Gaussian noise would be hard to justify. Prediction windows and critical-time windows would need a random error model and a method that accounts for dependence. No such model is made here, and no autoregressive correction is silently added and then claimed as part of the PDE.

Sensitivity of the Fitted Singularity and Forecast Ranking

Stability of the search and steadiness of forecasts are different ideas. The first test changes the largest allowed critical-time gap while keeping the training data the same. Table 5 shows the outcomes.

Table 5: Sensitivity to the maximum allowed critical-time gap

Maximum allowed gap (years)	Fitted gap (years)	Training RMSE	Withheld RMSE
5	1.574471	124.508	509.261
10	1.574471	124.508	509.261
20	1.574471	124.508	509.261
50	1.574471	124.508	509.261

Source: *Re-estimation of the profile objective (32) with the lower gap limit fixed at 0.60 calendar years. Only the upper search bound changes. Small differences in the final digits reflect numerical refinement.*

All four searches produce the same fitted gap and forecast errors. So the main estimate is not a result of picking a 20-year upper limit. This steadiness does not make the estimated singularity an actual economic date. It only shows that the same least-squares answer appears in all four search ranges.

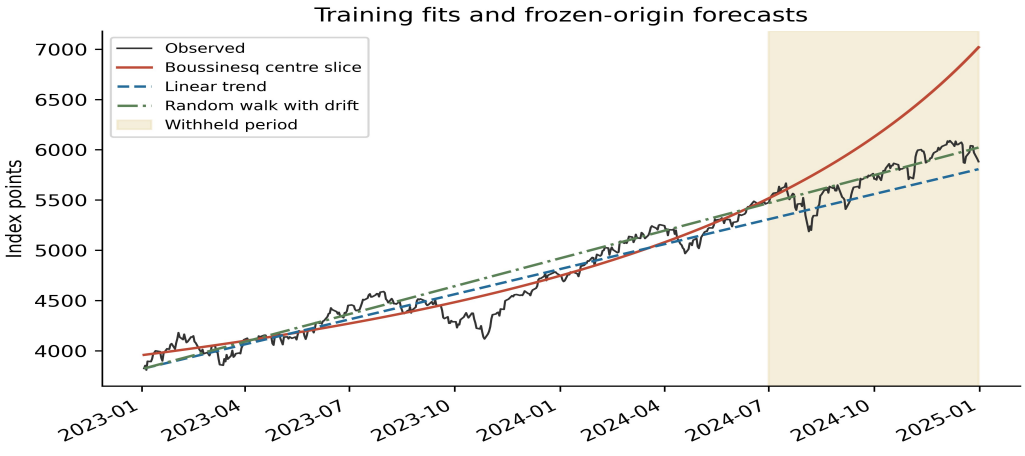


Figure 4: Training RMSE profiled over the critical-time gap.

Source: *Authors' calculations. The baseline and amplitude are re-estimated at every shown gap. The horizontal axis uses a log scale. The dashed line shows the lowest point of the profile. This is a profile of the objective function, not a confidence band.*

The second test uses expanding training sets that finish on 29 December 2023, 28 March 2024 and 28 June 2024. After each model is built, it forecasts the next 63 trading closes without changing the model. The Boussinesq fit keeps the critical-time gap limits. Table 6 shows the RMSE for each starting point.

Table 6: Forecast RMSE over the next 63 trading observations

Forecast Origin	Boussinesq Slice	Linear Trend	Random Walk	Walk With Drift
2023-12-29	306.94	317.36	282.97	140.91
2024-03-28	598.03	175.36	143.94	180.38
2024-06-28	304.53	162.52	148.25	136.31

Source: *Expanding-window re-estimation using observations available at each origin. Each row evluates 63 observations in index points. These are three origin checks, not an independent replication sample.*

The Boussinesq slice never has the lowest RMSE at any of these starting points. It does a little better than the trend at the December 2023 start, but it is worse than the random-walk and drift models. At the March 2024 start its error jumps up. At the June start it also does worse than all three models. So the result does not rely on the six-month window used in Table 4.

Because we only have three starting-point tests, we do not claim a clear winner or run a formal test of superiority. This work also does not look at trading profits, costs or risk-adjusted gains. The only conclusion is that the chosen singular solution branch did not give a better forecast than simple models in this example.

MEANING OF THE FINDINGS FOR SYMMETRY AND CONSERVATION

The data curve is linked to the main equation by a proven exact solution, which fixes the earlier problem of creating a PDE and then trying an unrelated AR(1) model. Still, having a solution does not mean the model is right for the data. The price data show a small piece of the whole field and leave many structural constants unknown.

The chosen polynomial solution does not decay over space. Its total mass and energy over all space are infinite. Because of that, the fit cannot be shown as a market calibration that follows conservation rules. We do not give a market-energy number that stays constant. The finite-energy travelling pulse that comes from the method is a different kind of solution; it moves with the same size all the time and cannot replace the growing polynomial solution unless we change how we look at the data.

The instability analysis of the bad Boussinesq equation stays separate from the other parts. The polynomial family has zero fourth spatial derivative, so the fitted curve does not hold any details about short-wavelength amplification controlled by β. Because of this, a good or bad scalar fit cannot alone reveal the stability properties of the financial interaction field.

Charlier et al. (2025) examine the treatment of the bad Boussinesq equation using mathematical reference solutions. The difference between equation verification and application validation is

also needed here. The current empirical exercise compares an observation curve with market data; it does not provide a solution of the unrestricted PDE initial-value problem.

Financial Interpretation and Practical Implications

The first implication is methodological. A rising price path can be described by smooth curves. The best interpretation must rely on evidence, identified parameters and the amount of unexplained variation. In this episode the singular curve's lower training error does not make up for its larger withheld forecast error.

The second implication deals with early-warning claims. The fitted T must not be presented as a predicted crash date. Its value depends on a solution branch, an observation location, a time window and an additive baseline. The data do not estimate a crash hazard or give a behavioural transition mechanism. Strong residual persistence adds another reason to be careful about point forecasts.

The third implication involves financial decision making. These results do not support replacing established risk monitoring with a singularity estimate. A useful warning system needs testing across episodes, also in times that do not finish with sharp corrections, so that false alarms and missed events can be measured. A persuasive curve fitted after a rally has already happened cannot create such a system.

Finally, future PDE applications need observations that explain the interaction coordinate. Cross-sectional sentiment, sector valuations or a defined network embedding could be candidates. Their measurement and mapping into the model must be justified. Additional variables must not be called evidence until they are collected and put into an estimation design.

Limitations and Boundaries of the Evidence

The study uses one equity index during one historical rally. It does not show behaviour across countries, asset classes, crashes or other macroeconomic regimes. Dividends are left out, so the observed changes are price-index changes instead of total returns. Missing published values are omitted without trying to guess trading activity.

The train/test split and the three origin checks are done after the fact. No competing PDE solution branch, LPPL specification, stochastic-volatility model or estimated autoregression is examined. Their absence stops a model ranking, even though it does not change the shown comparisons. No information criteria are given because the persistent regression discrepancies have not received a common independent-error likelihood.

The single observation series does not determine the PDE's coefficients, initial field or boundary conditions. The solution used for fitting is not localized in space, and conservation-law calibration is missing. The diagnostics show errors, and no proper stochastic uncertainty model has been added yet. Formal claims about parameter precision, forecast coverage or causal market feedback are therefore beyond the evidence.

The reproducibility archive logs the retrieved observations and their SHA-256 checksum, software versions, processing rules and analysis script. This lets the numerical results be verified without replacing data with made-up values. It does not lift the licensing conditions on the source series; redistribution or journal reproduction must follow the provider's stated terms.

CONCLUDING INTERPRETATION

The observed S&P 500 rally gives a real-data setting where the boom-phase analogy can be checked. The exact Boussinesq centre slice captures part of the rising training trajectory. Its accelerating extrapolation goes far beyond the withheld period. Drift and exponential forecasts do better, and the slice leaves strongly autocorrelated residuals.

The defensible conclusion is that this particular solution-based observation model has limits in explanation and does not beat benchmark forecasts in the studied episode. Symmetry reduction gives a functional form, but empirical evaluation shows where that form fails. More financial use of the Boussinesq framework needs an identified spatial observation model and wider validation, not stronger claims from the same single price path.

REFERENCES

Bluman, G. W., & Anco, S. C. (2002). *Symmetry and integration methods for differential equations*. Springer. https://doi.org/10.1007/b97380

Brocchini, M. (2013). A reasoned overview on Boussinesq-type models: The interplay between physics, mathematics and numerics. *Proceedings of the Royal Society A: Mathematical, Physical and Engineering Sciences*, 469(2160), Article 20130496. https://doi.org/10.1098/rspa.2013.0496

Charlier, C., Eriksson, D., & Lenells, J. (2025). Numerical scheme for the solution of the "bad" Boussinesq equation. *Applied Numerical Mathematics*, 217, 216–233. https://doi.org/10.1016/j.apnum.2025.06.011

Hyndman, R. J., & Athanasopoulos, G. (2021). *Forecasting: Principles and practice* (3rd ed.). OTexts. https://otexts.com/fpp3/

Johansen, A., & Sornette, D. (2001). Finite-time singularity in the dynamics of the world population, economic and financial indices. *Physica A: Statistical Mechanics and its Applications*, 294(3–4), 465–502. https://doi.org/10.1016/S0378-4371(01)00105-4

National Institute of Standards and Technology. (2023, December 11). Ljung–Box test. *Dataplot reference manual*. https://www.itl.nist.gov/div898/software/dataplot/refman1/auxillar/ljungbox.htm

Olver, P. J. (1993). *Applications of Lie groups to differential equations* (2nd ed.). Springer. https://doi.org/10.1007/978-1-4612-4350-2

S&P Dow Jones Indices LLC. (n.d.). *S&P 500 [SP500]* [Data set]. FRED, Federal Reserve Bank of St. Louis. Retrieved October 30, 2026, from https://fred.stlouisfed.org/series/SP500

APPENDIX

Audit of the Daily Observations

The following extract offers a concise audit of the daily dataset. It shows the final published trading close for each month and the count of trading days that have data. The full 502-row daily dataset is available in the reproducibility archive. Month-end percentage changes are differences between the month-end levels shown, not sums of daily log returns. The first month does not have a preceding month-end observation in the downloaded interval, so the comparison is left blank.

Table A1: Monthly audit extract from the retrieved series

Month	Trading date	Closing index	Trading observations	Month-end change (%)
2023-01	2023-01-31	4076.60	20	—
2023-02	2023-02-28	3970.15	19	−2.611
2023-03	2023-03-31	4109.31	23	3.505
2023-04	2023-04-28	4169.48	19	1.464
2023-05	2023-05-31	4179.83	22	0.248
2023-06	2023-06-30	4450.38	21	6.473
2023-07	2023-07-31	4588.96	20	3.114
2023-08	2023-08-31	4507.66	23	−1.772
2023-09	2023-09-29	4288.05	20	−4.872
2023-10	2023-10-31	4193.80	22	−2.198
2023-11	2023-11-30	4567.80	21	8.918
2023-12	2023-12-29	4769.83	20	4.423
2024-01	2024-01-31	4845.65	21	1.590
2024-02	2024-02-29	5096.27	20	5.172
2024-03	2024-03-28	5254.35	20	3.102
2024-04	2024-04-30	5035.69	22	−4.162
2024-05	2024-05-31	5277.51	22	4.802
2024-06	2024-06-28	5460.48	19	3.467
2024-07	2024-07-31	5522.30	22	1.132
2024-08	2024-08-30	5648.40	22	2.283
2024-09	2024-09-30	5762.48	20	2.020
2024-10	2024-10-31	5705.45	23	−0.990
2024-11	2024-11-29	6032.38	20	5.730
2024-12	2024-12-31	5881.63	21	−2.499

Source: *FRED SP500 observations, aggregated by the authors. These are month-end values, not average index levels. The total of the trading-observation counts is 502.*